Available online at www.sciencedirect.com

ScienceDirect

Mendeleev Commun., 2023, **33**, 368–371

Mendeleev Communications

Effect of synthesis conditions on morphology, crystal structure and electrochemical properties of β-NaV_6O_{15}

Olga I. Gyrdasova,* Elena V. Vladimirova, Larisa Yu. Buldakova, Mikhail Yu. Yanchenko and Alexandr V. Dmitriev

Institute of Solid State Chemistry, Ural Branch of the Russian Academy of Sciences, 620990 Ekaterinburg, Russian Federation. E-mail: Gyrdasova@ihim.uran.ru

DOI: 10.1016/j.mencom.2023.04.023

Current–voltage characteristics of nanostructured vanadium oxide bronze β-NaV_6O_{15} obtained from oxalate solutions by ultrasonic spray pyrolysis (USP) under various conditions were studied. The conditions of USP synthesis significantly affected the particle morphology, specific surface area, defect structure and oxidizing ability of the compound.

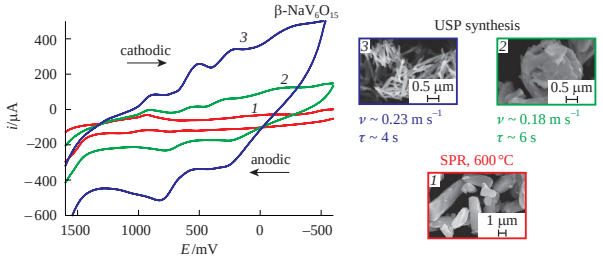

Keywords: vanadium oxide bronze, precursor synthesis, ultrasonic spray pyrolysis, voltammetry, chemisorption.

Vanadium oxides and compounds based on them exhibit a layered or tunnel type of crystal structure built from vanadium–oxygen coordination polyhedra, which ensures significant mobility of intercalated metal cations.[1] This feature makes them promising for use as chemical sensors, nanosized magnets, electrical and optical devices, sensor materials and electrodes for intercalation batteries.[2,3] Vanadium(V) oxide V_2O_5 has found particular practical application in the composition of cathode materials for metal-ion batteries, which demonstrate high energy density (charging capacity up to 650 mA h g^{-1}) and significant cycle stability.[3,4] The disadvantage of V_2O_5 is its low electrical conductivity, low diffusion coefficient of intercalated cations and structural instability during charging/discharging, which reduces its electrochemical characteristics.[5] Vanadium oxide bronze (VOB) NaV_6O_{15} (or β-$Na_{0.33}V_2O_5$) is chemically stable and has high electrical conductivity and charging capacity.[6,7] The typical tunnel structure of the vanadium–oxygen framework promotes the reversible introduction/removal of metal ions. The electrochemical behavior of a material largely depends on its surface, crystallite size and particle morphology. Many methods for the synthesis of NaV_6O_{15}, including the sol–gel method, chemical precipitation,[7,8] hydrothermal method[9] and solvothermal reaction,[10] have been used to improve its electrochemical characteristics.

When using these methods, crystallites have such morphological features as quasi-one-dimensionality and sphericity, among others. Many authors note excellent electrochemical characteristics for thin films and 3D structures with a high initial discharge capacity and performance retention after 30 operation cycles.[7–9] Of greatest interest is the production of oxide materials in the form of hollow microspheres, since these objects combine the advantages of 3D structures and thin films. Most of the works are devoted to obtaining V_2O_n microspheres. Nevertheless, obtaining complex oxides of the NaV_6O_{15} type in this form remains a problem. When producing hollow microspheres, template methods[11] and spray pyrolysis[12] are usually used. The authors of this work have large experience in the preparation of oxide compounds in the form of microspheres by ultrasonic spray pyrolysis (USP).[12,13] The USP method makes it possible to control the conditions for the formation of single-phase vanadium oxide from an aqueous aerosol with a radial distribution of dissolved components in the drop volume. This ensures the formation of spherical agglomerates of a given diameter.[13] The shell of such structures consists of nanocrystallites with an average size of 30–40 nm. By varying the intensity of ultrasonic treatment, the temperature and atmosphere of aerosol thermolysis, it is possible to obtain vanadium oxide compounds in the expected valence and morphological state. An urgent research task is to establish a relationship between the conditions for obtaining complex oxides and the nature of defect centers. The method of voltammetry makes it possible to establish the relationship between the degree of defectiveness of the obtained VOB samples and their electrochemical activity.

In this work, β-NaV_6O_{15} was obtained by USP in the form of quasi-one-dimensional and hollow microspheres and the influence of USP synthesis conditions on the morphology, crystal structure and electrochemical properties was investigated. Samples of β-NaV_6O_{15} were synthesized in the previously described USP setup[12] with a sputtering frequency of 1.7 MHz. The working solution was an aqueous solution of stoichiometric amounts of NH_4VO_3 (c.p.) and Na_2CO_3 (c.p.). Oxalic acid $H_2C_2O_4$ (e.c.) was used as the carboxylic acid. The addition of carboxylic acids ensures the reduction of VO_3^- to VO^{2+} ions and contributes to the stabilization of the vanadyl ion in the aqueous medium:[13,14]

$$2VO_3^- + 4H_2C_2O_4 = [(VO)_2(C_2O_4)_3]^{2-} + 2CO + 4H_2O,$$

$$[(VO)_2(C_2O_4)_3]^{2-} + Na^+ = Na[(VO)_2(C_2O_4)_3]^-.$$

Synthesis under USP conditions occurs in one microdroplet of the solution in the time required to cover a distance equal to the length of the reactor with the speed of supply of the carrier gas. Important factors for determining the phase composition and morphology of the resulting product are the concentration of the initial solution ($C_{V^{4+}}$), the synthesis temperature (T) and the synthesis time (τ), which is determined by the aerosol feed rate

© 2023 Mendeleev Communications. Published by ELSEVIER B.V. on behalf of the N. D. Zelinsky Institute of Organic Chemistry of the Russian Academy of Sciences.

Table 1 Effect of USP synthesis conditions on the phase composition of the samples.

Sample	$C_{V^{4+}}$/mol dm^{-3}	ν/m s^{-1}	τ/s	T/°C	Phase composition (wt%)
a	0.05	0.1755	5.7	600	$NaV_{6-x}O_{15}$ (57) + VO_2 (43)
b	0.10	0.2295	4.3	600	$NaV_{6-x}O_{15}$ (86) + VO_2 (14)
I	0.05	0.2295	4.3	650	NaV_6O_{15} (100)
II	0.05	0.1755	5.7	650	NaV_6O_{15} (100)

(ν). The experimentally determined USP conditions are given in Table 1. Figure 1 shows the X-ray diffraction patterns of the synthesized samples.† In all cases, the peaks corresponding to β-NaV_6O_{15} are clearly expressed (ICSD card no. 086-0120). Samples obtained at a temperature of 600 °C contain the impurity of VO_2 (ICSD card no. 019-1398). Moreover, the amount of VO_2 in sample **a** prepared from a less concentrated solution is 43% (see Figure 1). The use of a more concentrated solution reduces the content of the VO_2 impurity in sample **b** to 14% (see Figure 1).

According to experimental data, it is possible to obtain single-phase samples of β-NaV_6O_{15} by the USP method from solutions with $C_{V^{4+}}$ = 0.05 mol dm^{-3} at a temperature of T = 650 °C. Changing the aerosol feed rate does not affect the phase composition of the product, but significantly affects the particle morphology. The unit cell parameters of single-phase samples are given in Table 1.

Sample **III** of β-NaV_6O_{15} was obtained as a standard by solid phase reaction (SPR) at 600 °C from V_2O_5 (h.c.) and Na_2CO_3 (e.c.). Single-phase samples **I**–**III** were selected for further studies. X-ray diffraction patterns indicate a monoclinic system (space group $A2/m$) with unit cell parameters given in Table 2.

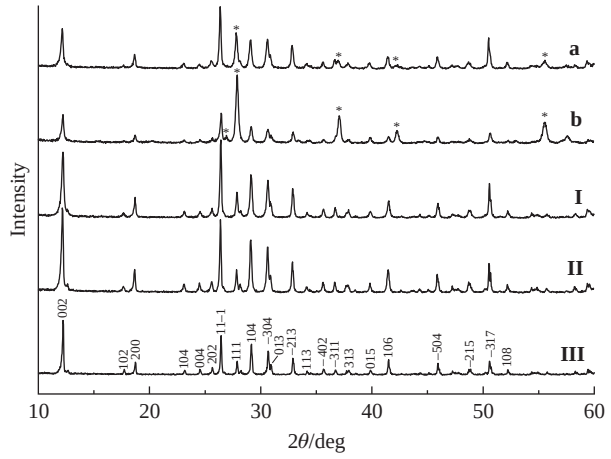

Figure 1 X-ray diffraction patterns of NaV_6O_{15} prepared under either USP conditions (samples **a**, **b**, **I** and **II**) or SPR conditions (sample **III**). VO_2 admixture peaks are marked with an asterisk.

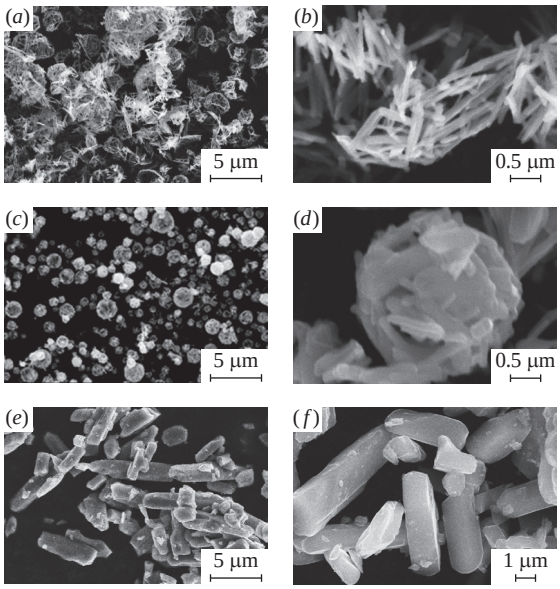

Figure 2 SEM images of various NaV_6O_{15} samples: (*a*),(*b*) **I**, (*c*),(*d*) **II** and (*e*),(*f*) **III**.

It can be seen that the change in the unit cell parameters is insignificant. A slight increase in parameter c and unit cell volume V for sample **I** indicates an increase in the interlayer distance of the vanadium–oxygen framework, which promotes the intercalation of metal cations (for example, lithium in lithium-ion batteries) into the β-NaV_6O_{15} structure. Figure 2 shows the SEM images‡ of the particles of all NaV_6O_{15} samples.

Samples obtained under USP conditions are spherical agglomerates consisting of quasi-one-dimensional particles (whiskers). Sample **I** of the NaV_6O_{15} compound was obtained with a short synthesis time in the form of quasi-one-dimensional particles 0.8 μm long and 0.1 μm thick. An increase in the synthesis time leads to thickening of the quasiparticles due to longitudinal intergrowths (sample **II** of the NaV_6O_{15} compound). Simultaneously, the formation of dense spherical agglomerates with a diameter of 1 to 3 μm is observed. Unlike sample **I** of the NaV_6O_{15} compound, in which most of the spheres are destroyed, sample **III** of the NaV_6O_{15} compound obtained under static conditions consists of well-crystallized massive particles about 5 μm long and 1–1.5 μm thick. The CSR values (see Table 2) also indicate an increase in the crystallite size in the series of NaV_6O_{15} samples **I**, **II** and **III**. Samples **II** and **III** have comparable values of specific surface area, while the surface of sample **I** exceeds that of other samples by almost a factor of two (see Table 1).

The obtained voltammetry data§ characterize the redox processes on the surface of the samples under study (cathodic polarization)

Table 2 Main characteristics of single-phase samples of β-NaV_6O_{15}.

Sample	Synthesis method	T/°C	τ/s	Lattice parameters/Å			β/deg	V/Å^3	CSR/nm	Particle size/μm		BET area/m^2 g^{-1}	BJH adsorption pore volume/cm^3 g^{-1}
				a	b	c				Length	Width		
I	USP	650	4.4	10.0709	3.6072	15.4039	109.58	527.23	52	0.8	0.1	12.01	0.036
II	USP	650	5.7	10.0724	3.6064	15.3908	109.53	526.91	62	1.0	0.2	7.65	0.027
III	SPR	600	21600	10.0708	3.6072	15.3939	109.54	527.01	76	5.3	1.4	6.44	0.014

† Powder X-ray diffraction patterns were obtained at room temperature on a Shimadzu XRD-7000 diffractometer with a secondary monochromator using CuKα radiation in the 2θ angle range from 10 to 80° in 0.03° increments.

‡ The morphological features of the samples were examined by scanning electron microscopy (SEM) on a JEOL JSM 6390 LA microscope (magnification factor from 5× to 300 000×, resolution 3.0 nm at 30 kV) with an EDS Inca Energy 250 X-ray spectrometer. Porosity was determined by the low-temperature (77 K) nitrogen sorption on a Micromeritics Gemini VII Surface Area and Porosity 2390t analyzer.

§ To study the voltammetric behavior of the samples, a carbon paste electroactive electrode (CPEE) with a visible surface area of 0.047 cm^2

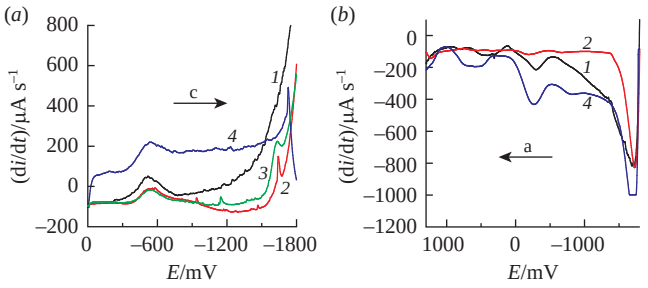

Figure 3 (*a*) Cathodic (c) and (*b*) anodic (a) branches of differential voltammograms of (*1*) V_2O_5 and NaV_6O_{15} samples: (*2*) **III**, (*3*) **II** and (*4*) **I**.

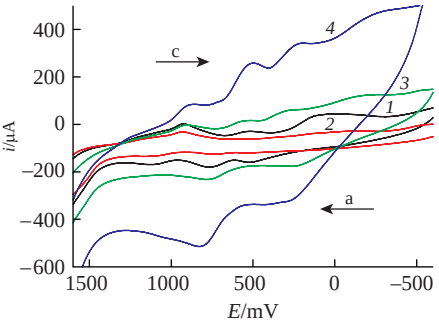

Figure 4 Integrated cathode–anode voltammograms of oxygen chemisorbed on (*1*) V_2O_5, (*2*) NaV_6O_{15} sample **III**, (*3*) NaV_6O_{15} sample **II** and (*4*) NaV_6O_{15} sample **I**.

and electrochemical discharge with surface oxygen chemisorption (anodic process). On the cathodic branch of the V_2O_5 voltammogram, a number of successive peaks of reduction of the surface layer of vanadium(V) oxide were registered at potentials E_1 = −460 mV ($V^{5+} \rightarrow V^{4+}$), E_2 = −680 mV (shoulder of the reduction peak $V^{4+} \rightarrow V^{3+}$) and E_3 = −1600 mV ($V^{3+} \rightarrow V^{2+}$) [Figure 3(*a*)].

The V^{2+} reduction wave merges with the hydrogen reduction wave. Signals of reverse transformations are recorded on the anodic branch of the voltammogram [Figure 3(*b*)]: at the maximum potential E_1 = −800 mV, a blurred peak is seen for the oxidation process $V^{2+} \rightarrow V^{3+}$, and then at the potential E_2 = −250 mV and in the potential range of 500–700 mV, there are peaks for the processes $V^{3+} \rightarrow V^{4+}$ and $V^{4+} \rightarrow V^{5+}$, respectively. The curves for V_2O_5 correspond to those previously described.[15] Similar signals of sequential reduction/oxidation of vanadium were recorded in the voltammograms of the VOB samples, which indicates a predominantly pentavalent state of vanadium in the β-NaV_6O_{15} structure. The magnitudes of the reduction currents of NaV_6O_{15} (sample **III**) are comparable to those for V_2O_5. The vanadium reduction currents for samples **I** and **II** are much higher in magnitude than for sample **III**. In addition, the shift of the main maxima of the reduction peaks, which is especially significant in the $V^{3+} \rightarrow V^{2+}$ reaction for NaV_6O_{15} samples **I** and **II**, to the region of negative values indicates an increase in oxidative activity in the series NaV_6O_{15} (sample **III**) → NaV_6O_{15} (sample **II**) → NaV_6O_{15} (sample **I**). Electrochemical transformations of chemisorbed oxygen are directly associated to the defective structure of oxides and make it possible to predict the catalytic activity of compounds.[15,16] In the framework of quasi-chemical concepts, the equilibrium between oxygen in the liquid and oxide lattice defects can be shown by the equations:

$$O_o = V_O^{+} + \bar{e} + O^{-},$$

$$O_o = V_O^{2+} + 2\bar{e} + O^{-}.$$

We have studied the process of oxygen chemisorption on the surface of the entire NaV_6O_{15} sample. The electrode containing the test sample was pre-exposed at a potential exceeding the water decomposition potential. The oxygen released in this case was chemisorbed by the NaV_6O_{15} surface. On the cathodic branches of the voltammograms of V_2O_5 and the studied VOB in the potential range of 0–1000 mV, several signals of the reduction of various forms of chemisorbed oxygen were recorded. The reduction current values vary depending on the sample preparation method and are maximum for NaV_6O_{15} (sample **I**), which has a more developed surface (Figure 4).

This may be due to the largest number of defects in the sample.[17] For this sample, peak potentials also shifted by 100 mV to the region of negative potentials for the cathodic branch and by 100 mV to the region of positive potentials for the anodic branch, which indicates an increase in the binding energy of surface defects with chemisorbed oxygen. The peak characteristic of V_2O_5 at 100 mV for NaV_6O_{15} samples **I** and **II** split into two peaks at 250 and −150 mV. To determine the kinetic parameters of the oxidation/reduction processes of V_2O_5 and VOB, a logarithmic dependence of the current value in a particular peak on the potential scan rate was plotted. In cyclic voltammetry, when determining the nature of

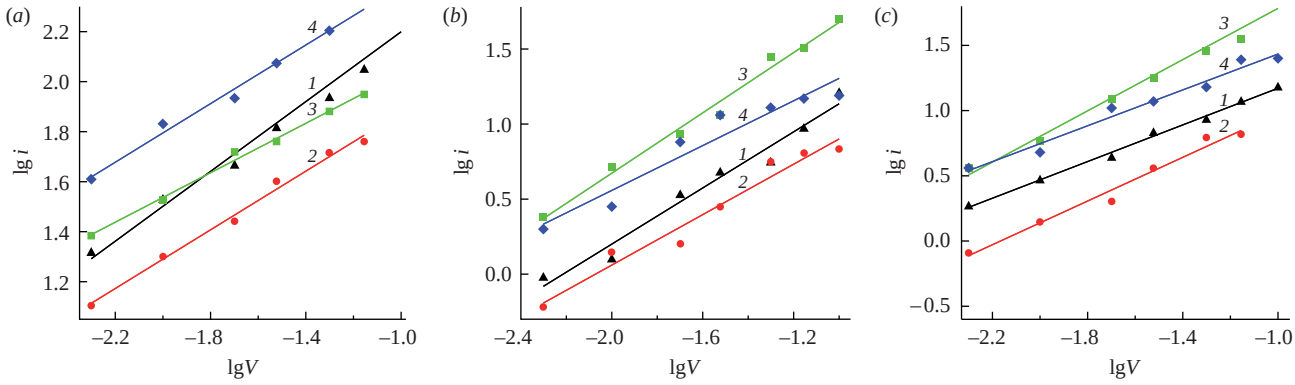

Figure 5 Logarithmic dependence of the peak current values at potentials (*a*) E_1, (*b*) E_2 and (*c*) E_3 on the potential sweep rate for (*1*) V_2O_5, (*2*) NaV_6O_{15} sample **III**, (*3*) NaV_6O_{15} sample **II** and (*4*) NaV_6O_{15} sample **I**.

was used as an indicator electrode. The electrode consisted of a mixture of the compound under study, spectroscopically pure graphite and mineral oil as a binder, taken in a mass ratio of 1 : 9 : 3, respectively. To standardize the CPEE surface, a graphite fraction with a particle size of ⩽ 63 μm was chosen. Saturated silver chloride electrodes EVL-1M3 served as the auxiliary and reference electrodes. A 0.5 M solution of Na_2SO_4 and a 0.1 M solution of H_2SO_4 were used as the background electrolyte.

To study the redox transformations of the initial samples, the cathodic potential sweep from 0 to −1800 mV was first set, then the sweep direction was changed and the anodic branch of the curve was recorded in the potential range from −1800 to 1200 mV. In the case of studying oxygen chemisorption, the indicator electrode was kept in solution at a potential of E = 1800 mV for 30 s (to release oxygen from the background electrolyte), then a voltammogram from 1800 to −700 mV was recorded.

currents, the Semerano criterion is used, which is found from the dependence:[18]

$$\lg ik = \lg V + \text{const},$$

where ik is the limiting current and V is the potential scan rate.

The linear dependence of the limiting current on the scan rate indicates the effect of adsorption on the electron transfer process. The tangent of the slope angle of the graph allows us to determine the limiting stage that determines the magnitude of the current in the peak: for diffusion processes $(\lg ik)/(\lg V) \approx 0.5$, for adsorption processes ~1. For the first reduction wave at E_1 in the range from –600 to –670 mV, the values of the Semerano coefficients characterize the course of a process close to diffusion [Figure 5(*a*)].

The value of $(\lg ik)/(\lg V)$ for V_2O_5 is 0.65, and for NaV_6O_{15} samples it varies from 0.49 to 0.55. According to published data,[15,16] in the range of 650–700 mV, the surface layer of V_2O_5 is reduced to VO^{2+}. The change in the values of the Semerano criterion for two subsequent waves of reduction of chemisorbed oxygen at E_2 = 600–670 mV and E_3 = −50 mV indicates a change in the limiting stage of the processes occurring during the electrochemical reaction. The values of the Semerano coefficients for the 2nd and 3rd waves are in the range of 0.80–0.90, which confirms the process controlled by adsorption [Figure 5(*b*),(*c*)].

Thus, the conditions for the synthesis of VOB, which determine the specific surface area and morphology of the particles, affect the electrochemical properties of the samples. Vanadium oxide bronze β-NaV_6O_{15} (sample **I**) with needle morphology of aggregates, obtained by the USP method, is characterized by increased oxidative activity and the binding energy of surface defects with chemisorbed oxygen. The established dependences indicate the prospects for using this compound as an electrode material and a catalyst for the oxidation of toxic organic impurities.

This work was carried out within the framework of the state assignment and research plans of the Institute of Solid State Chemistry of the Ural Branch of the Russian Academy of Sciences (grants nos. AAAA-A19-119031890025-9 and AAAA-A19-119031890026-6).

References

1 P. Y. Zavalij and M. S. Whittingham, *Acta Crystallogr., Sect. B: Struct. Sci.*, 1999, **55**, 627.
2 E. Strelcov, Y. Lilach and A. Kolmakov, *Nano Lett.*, 2009, **9**, 2322.
3 F. F. C. Bazito and R. M. Torresi, *J. Braz. Chem. Soc.*, 2006, **17**, 627.
4 M. M. Petrov, A. D. Modestov, D. V. Konev, A. E. Antipov, P. A. Loktionov, R. D. Pichugov, N. V. Kartashova, A. T. Glazkov, L. Z. Abunaeva, V. N. Andreev and M. A. Vorotyntsev, *Russ. Chem. Rev.*, 2021, **90**, 677.
5 Y. Cheng, X. Wang, S. Huang, W. Samarakoon, S. Xi, Y. Ji, H. Zhang, F. Zhang, Y. Du, Z. Feng, S. Adams and Q. Wang, *ACS Energy Lett.*, 2019, **4**, 3028.
6 J. Chen, H.-Y. Xu, J.-H. Ruan, Y.-M. Xin, Y. Li, D.-C. Li, A.-G. Wang and D.-S. Sun, *Mater. Chem. Phys.*, 2020, **249**, 122935.
7 S. Islam, M. H. Alfaruqi, B. Sambandam, D. Yunianto Putro, S. Kim, J. Jo, S. Kim, V. Mathew and J. Kim, *Chem. Commun.*, 2019, **55**, 3793.
8 M. Najdoski, V. Koleva, S. Stojkovikj and T. Todorovski, *Surf. Coat. Technol.*, 2015, **277**, 308.
9 M. Zhao, W. Zhang and X. Song, *Dalton Trans.*, 2017, **46**, 3857.
10 Q. Tan, Q. Zhu, A. Pan, Y. Wang, Y. Tang, X. Tan, S. Liang and G. Cao, *CrystEngComm*, 2015, **17**, 4774.
11 X. Zhang, J.-G. Wang, H. Liu, H. Liu and B. Wei, *Materials*, 2017, **10**, 77.
12 A. V. Dmitriev, E. V. Vladimirova, M. V. Kandaurov, A. Yu. Chufarov and D. G. Kellerman, *Phys. Solid State*, 2017, **59**, 2360 (*Fiz. Tverd. Tela*, 2017, **59**, 2338).
13 E. V. Vladimirova, O. I. Gyrdasova and A. V. Dmitriev, *Nanosyst.: Phys., Chem., Math.*, 2020, **11**, 572.
14 I. V. Baklanova, V. D. Zhuravlev, A. P. Tyutyunnik, M. A. Melkozerova and T. A. Patrusheva, *Mendeleev Commun.*, 2021, **31**, 723.
15 V. A. Blagojevic, J. P. Carlo, L. E. Brus, M. L. Steigerwald, Y. J. Uemura, S. J. L. Billinge, W. Zhou, P. W. Stephens, A. A. Aczel and G. M. Luke, *Phys. Rev. B: Condens. Matter Mater. Phys.*, 2010, **82**, 094453.
16 V. L.Volkov and L. Yu. Buldakova, *Elektrokhimiya*, 1994, **30**, 892 (in Russian).
17 G. S. Zakharova, L. Yu. Buldakova, V. L.Volkov, L. S. Molochnikov and E. G. Kovaleva, *Russ. J. Electrochem.*, 2006, **42**, 53 (*Elektrokhimiya*, 2006, **42**, 61).
18 G. K. Budnikov, V. N. Maistrenko and M. R. Vyaselev, *Osnovy sovremennogo elektrokhimicheskogo analiza* (*Fundamentals of Modern Electrochemical Analysis*), Mir, Moscow, 2003 (in Russian).

Received: 6th September 2022; Com. 22/6993